FISEVIER

Contents lists available at ScienceDirect

Journal of Colloid and Interface Science

journal homepage: www.elsevier.com/locate/jcis



Regular Article

High capacity aqueous phosphate reclamation using Fe/Mg-layered double hydroxide (LDH) dispersed on biochar



Sharifur Rahman ^{a,1}, Chanaka M. Navarathna ^{a,1}, Naba Krishna Das ^a, Jacinta Alchouron ^b, Parker Reneau ^c, Sean Stokes ^a, Rooban V.K.G. Thirumalai ^d, Felio Perez ^e, E. Barbary Hassan ^f, Dinesh Mohan ^g, Charles U. Pittman Jr. ^a, Todd Mlsna ^{a,*}

- ^a Department of Chemistry, Mississippi State University, Mississippi State, MS 39762, USA
- ^b Universidad de Buenos Aires, Facultad de Agronomía, Departamento de Recursos Naturales y Ambiente, Cátedra de Botánica General, Av. San Martín 4453, C1417DSE Buenos Aires, Argentina
- ^c Department of Chemical Engineering, Louisiana Tech University, Ruston, LA 71272, USA
- ^d Institute of Imaging and Analytic Technology (I²AT), Mississippi State University, Mississippi State, MS 39762, USA
- ^e Material Science Lab, Integrated Microscopy Center, University of Memphis, Memphis, TN 38152, USA
- f Department of Sustainable Bioproducts, Mississippi State University, Box 9820, Mississippi State, MS 39762, USA
- g School of Environmental Sciences, Jawaharlal Nehru University, New Delhi 110067, India

HIGHLIGHTS

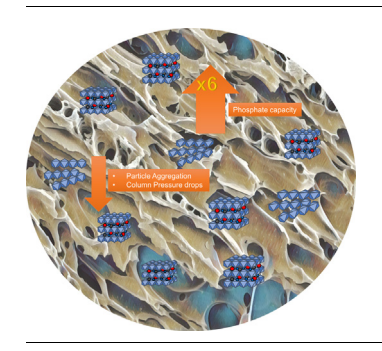
- Fe/Mg-LDH was dispersed on commercial high surface area Douglas fir biochar (LDHBC).
- LDHBC phosphate capacity (1279 mg/g) was six-fold greater than LDH (234 mg/g).
- 1 M NaOH stripped phosphate but reduced following P uptake.
- Ion-exchange, chemisorption and precipitation mechanisms were considered.

ARTICLE INFO

Article history: Received 27 December 2020 Revised 17 March 2021 Accepted 21 March 2021 Available online 24 March 2021

Keywords: Layered double hydroxide Phosphate Eutrophication Biochar Adsorption

G R A P H I C A L A B S T R A C T



ABSTRACT

Phosphate is a primary plant nutrient, serving integral role in environmental stability. Excessive phosphate in water causes eutrophication; hence, phosphate ions need to be harvested from soil nutrient levels and water and used efficiently. Fe-Mg (1:2) layered double hydroxides (LDH) were chemically co-precipitated and widely dispersed on a cheap, commercial Douglas fir biochar (695 m^2/g surface area and 0.26 cm^3/g pore volume) byproduct from syn gas production. This hybrid multiphase LDH dispersed on biochar (LDHBC) robustly adsorbed (~5h equilibrium) phosphate from aqueous solutions in exceptional sorption capacities and no pH dependence between pH 1–11. High phosphate Langmuir sorption capacities were found for both LDH (154 to 241 $\mathrm{mg/g}$) and LDH-modified biochar (117 to 1589 $\mathrm{mg/g}$). LDHBC was able to provide excellent sorption performance in the presence of nine competitive anion contaminants (CO_3^2 -, AsO_4^3 -, SeO_4^2 -, NO_3 , $\mathrm{Cr}_2\mathrm{O}_7^2$ -, Cl^- , F^- , SO_4^2 -, and MoO_4^2 -) and also upon remediating natural eutrophic water samples. Regeneration was demonstrated by stripping with aqueous 1 M NaOH. No dramatic performance drop was observed over 3 sorption-stripping cycles for low concentrations (5 ppm). The adsorbents and phosphate-laden adsorbents were characterized using Elemental analysis, BET, PZC, TGA, DSC, XRD, SEM, TEM, and XPS. The primary sorption mechanism is ion-exchange from low to moderate concentrations (10–500 ppm). Chemisorption and stoichiometric phosphate compound

E-mail address: TMlsna@chemistry.msstate.edu (T. Mlsna).

^{*} Corresponding author.

¹ These authors have made an equal contribution.

formation were also considered at higher phosphate concentrations (>500 ppm) and at 40 °C. This work advances the state of the art for environmentally friendly phosphate reclamation. These phosphate-laden adsorbents also have potential to be used as a slow-release phosphate fertilizer.

© 2021 Elsevier Inc. All rights reserved.

1. Introduction

Agricultural pollutants released into water bodies pose a serious problem to environmental stability. Excess phosphates from fertilizer runoff accumulate in water becoming a primary eutrophication source leading to dead zones (e.g. U.S. East Coast and the Gulf of Mexico) [1]. Phosphates are often the limiting reagent (<100 μg/L) for explosive algal growth [1]. Increased algae growth can reduce oxygen concentration in water, and release soluble neurotoxins and hepatotoxins by cyanobacteria blooms, and their ingestion can cause fish or livestock death and serious health effects in humans [2]. According to NOAA, 65% of coastal waters and estuaries are moderately to severely damaged by eutrophication. Due to the dense growth of blue green algae and hyacinthlike plants, short-term and long-term ecological effects are possible [3,4]. The total phosphorous (P) concentration in common raw domestic wastewater is ~10 mg/L [5]. Maximum P discharge limits (in US) in municipal treatment plant effluents are 1 and 0.5 mg/L P for discharge into the Upper Great Lakes into the Lower Great Lakes respectively [6].

Electrocoagulation [7], chemical precipitation [8], ion-exchange [9] and crystallization [10] have been used to remediates phosphate. These methods can be expensive and may not efficiently remediate phosphate. Also, chemical precipitation is complex and produces sludge.

The Fe-Mg (1:2 M ratio) LDH used in this study was previously modified by zwitterionic glycine to achieve good arsenate, phosphate and chromate adsorption capacities [20]. It was also used to remove uranium [21]. To best of our knowledge, no reports exist of dispersing of small LDH particles on high surface area larger particles to (1) permit suitable flow rates through packed columns, (2) prevent LDH particle aggregation, (3) obtain higher capacities and faster sorption rates, while, simultaneously (4) providing additional carbonaceous surfaces to remove additional sorbates. This Fe-Mg layered double hydroxide-modified biochar (LDHBC) is now used here to recover phosphate from aqueous solutions in high capacities.

The biochar (BC) used in this study is a commercially available, cheap, high surface area, large pore volume, carbon-rich adsorbent with a stable and long life carbon matrix [22] and a rough porous exterior. This BC is a byproduct of wet wood fast pyrolysis in an updraft gasifier at 900–1000 °C (1–10 s) under oxygen-starved conditions. BCs are now acceptable sorbents for metal cations

and organic sorbates [23]. This Douglas fir biochar and its nanomodified (metal oxides, metal organic frameworks, etc.) hybrid composite analogs were previously employed to sorb of heavy metals [24], pesticides [25], pharmaceuticals [26], oxyanions [27], dyes [28] and oils [23]. Recently, we reported that Fe₃O₄ nanoparticles dispersed on Douglas fir biochar gave excellent aqueous phosphate removal [5].

A high Fe-Mg LDH surface area was achieved by its dispersion on the BC surface to make LDHBC. Fe-Mg LDH is the primary adsorption phase for aqueous phosphate. Superior batch and fixed-bed column remediations were achieved along with the highest phosphate capacities ever previously reported for neat biochar or Fe-Mg LDH in the literature. The biochar's surface only adsorbs a very small amount of phosphate [5]. This enables the clear view of how the phosphate sorption of LDH compares with LDHBC. Phosphate adsorption was studied versus pH, equilibrium time, phosphate concentrations, adsorbent doses, temperatures, the presence of co-existing competitive contaminants, and in more complex eutrophic systems. Sorption mechanistic considerations were supplemented by an X-Ray photoelectron spectroscopy (XPS) study.

2. Experimental

2.1. Reagents and equipment

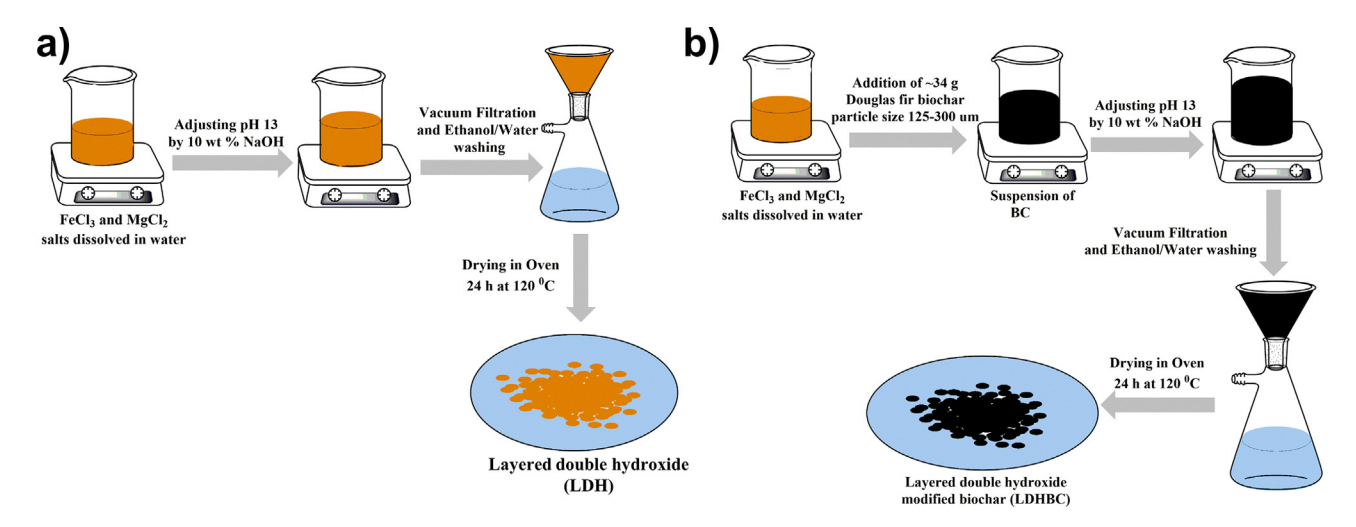
All chemicals used were Analytical grade. Chemicals were purchased from Sigma-Aldrich (St. Louis, MO) unless otherwise specified. Stock solutions (2.5 to 1000 mg/L) of phosphate were made by dissolving KH₂PO₄ in de-ionized water from a Millipore-Q water system. The pH measurements were made using a Hanna pH/ORP Meter and test solution pHs were adjusted using either 0.01, 0.1 and 1 M HCl or NaOH. Adsorption studies were conducted in an Orbital shaker (Thermo Forma) or in an incubating shaker. Phosphate sample concentrations were determined using ascorbic acid colorimetry using UV-Vis Spectrometer at 820 nm wavelength.

2.2. Biochar

Biochar (BC) (supplied by Biochar Supreme, Everson, WA) is a by-product from the wet wood gasification of waste Douglas fir timber. Chipped ($\sim\!\!3$ in.), auger fed, green wood was feed to an air-fed updraft gasifier (at 900 – 1000 °C) with a 1–10 s residence time. Large biochar particles ($\sim\!\!2$ cm) were water washed several times to remove fine particulates, water soluble organic compounds, and other impurities. Washed particles were dried at room temperature (2–3 days), ground, sieved to 150–300 μm size range and stored in closed vessels for use in all adsorption studies.

2.3. Preparation of layered double hydroxides (LDH) and modified douglas fir biochar (LDHBC)

Fe/Mg-LDH was synthesized in a 1:2 Fe $^{3+}$: Mg $^{2+}$ molar ratio. Aqueous iron (III) chloride (\sim 12.2 g) and magnesium chloride hexahydrate (\sim 30.6 g) was dissolved in \sim 200 mL de-ionized water. This pH was raised to 13 by dropwise addition of a 10% aqueous NaOH (Scheme 1a). This solution was stirred for 24 h at 25 °C, vacuum filtered to remove Fe/Mg LDH, and this solid was subsequently



Scheme 1. Preparation of a) LDH and b) LDHBC.

washed with ethanol (\sim 100 mL) and water (\sim 200 mL). After oven drying at 120 °C for 24 h, Fe/Mg LDH was obtained. LDHBC was prepared using the same method (Scheme 2b) by slurring \sim 34 g of Douglas fir BC (particle size 125–300 μ m) in the aqueous iron and magnesium salt solution. The weights of LDH and LDHBC obtained were \sim 19.8 g and \sim 46 g, respectively. Both adsorbents were sieved to particle sizes 125–300 μ m and stored in polypropylene containers until further use.

LDH, LDHBC and their P-laden analogues were extensively characterized. Experimental details describing point of zero charge (PZC) measurements, thermogravimetric analysis (TGA) and differential scanning calorimetry (DSC), scanning electron microscopy (SEM) and energy dispersive analysis by X-ray (EDX, transmission electron microscopy (TEM) and energy-dispersive analysis by X-ray (EDX), X-ray diffraction (XRD) and Xray photoelectron spectroscopy (XPS), surface area measurement and proximate and ultimate analysis are given in the supporting material.

2.4. Batch sorption studies

Aqueous solutions of 50 mg/L phosphate (25.0 mL) were used to study how pH effects adsorption onto LDH and LDHBC (25.0 mg). We studied phosphate sorption onto pristine BC previously [5], and the uptake was negligible. Hence, it was not tested here. Solution pH values were adjusted to pH 1, 3, 5, 7, 9, 11 and 13 using 1 M, 0.1 M, and 0.01 M of HCl and NaOH. A pH of 7 was chosen for kinetic and isotherm experiments because it is closer to water's natural pH of water. Phosphate removal remained almost constant for both LDH and LDHBC over the experimental pH range.

Sorption kinetics of both LDH and LDHBC were studied using 50 mg doses of LDH or LDHBC with 25 mL of phosphate at concentrations of 50, 100 and 500 mg/L, at pH 7 and 25 °C. The containers were shaken in an orbital shaker at 200 rpm for specific times [30 s, (1, 1.5, 2, 3, 4, 5, 8, 10, 15, 30, 45, 60) mins and (2, 3, 4, 5, 6, 12 and 24) h], filtered through a 0.22 μm filter and then analyzed for phosphate.

Batch isotherm experiments employed 2.5 to 2500 mg/L aqueous phosphate solutions (25.0 mL), equilibrated with either LDH or LDHBC (50.0 mg) at pH 7 and at 10, 25 and 40 °C. Phosphate concentrations remaining in the filtrate were analyzed by the ascorbic acid colorimetry method [29] using a double beam UV–Visible spectrophotometer (820 nm). Phosphate adsorption per unit of adsorbent (q_e) is given by Eq. (1).

$$q_e = \frac{V(C_0 - C_e)}{M} \tag{1} \label{eq:qe}$$

Here, C_0 and C_e (mg/L) are initial and equilibrium solution phosphate concentrations, V (L) is the volume (25.0 mL), and M (g) is the total mass of adsorbent. All experiments were triplicated.

2.5. Assessing suitability for applied water treatment

2.5.1. Ion competition

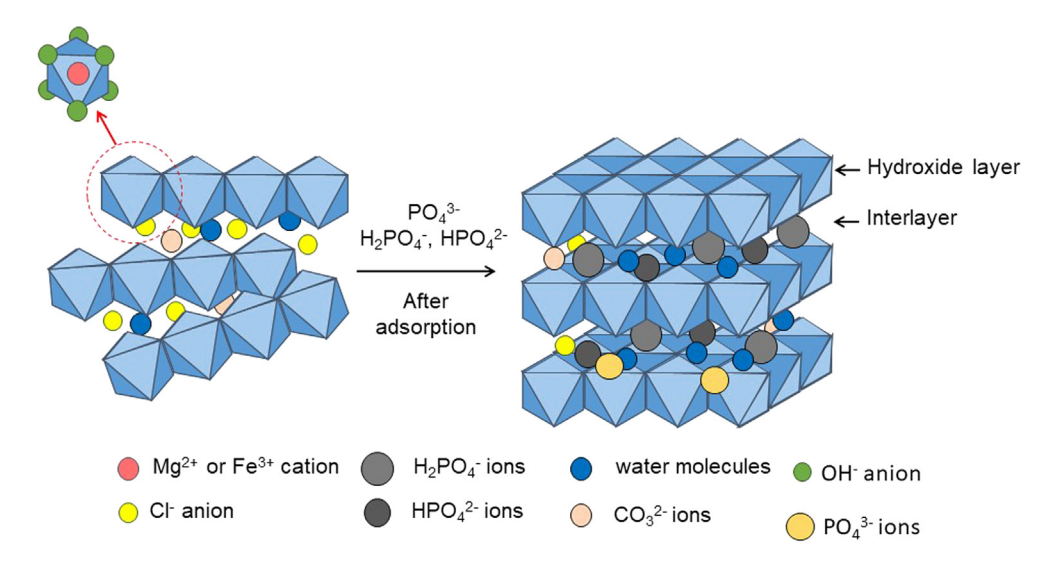
Phosphate sorption onto LDHBC was investigated in the presence of CO_3^{2-} , AsO_4^{3-} , SeO_4^{2-} , NO_5 , $Cr_2O_7^{2-}$, Cl^- , F^- , SO_4^{2-} , and MoO_4^2 . Ion selection was based on the 1) similar chemistry to phosphate (arsenate, dichromate, selenate, molybdate and sulphate) and 2) their habitual presence in natural waters (nitrate, chloride, carbonate and fluoride). At first, the effect of each individual competing ion was explored at three different concentrations (0.01, 0.1 and 1 mM) with 50 mg/L PO_4^{3-} . Then, their simultaneous effect over phosphate adsorption was studied by mixing all of them together at three different concentrations (0.01, 0.1 and 1 mM) to three separate solutions containing 50 mg/L PO_4^{3-} . All experiments were triplicated, equilibrating 50 mg of LDHBC with 25 mL of solutions at 25 °C, for 24 hrs at 200 rpm. Post agitation, mixtures were filtered, and remaining phosphate concentrations were determined.

2.5.2. Application of LDHBC for eutrophic lake and pond water treatment

LDHBC's sorption performance in an authentic eutrophic water was investigated by water collected from Chadwick Lake, Mississippi State, MS 39762 and Eckie's Pond, Mississippi State, 39759. Water samples were filtered through Whatman filter paper (Number 1, CAT No. 1001–110, pore size: 11 μm). Phosphate contents and pH of the Lake and pond water samples were determined. LDHBC (25 mg) were then added to each of these samples (25 mL) and equilibrated for 6 h. Subsequently, lake water and distilled water were adjusted to pH 7 and the sorption experiments were repeated.

2.5.3. Regeneration procedure

Stripping regeneration of LDHBC were performed using 1 M NaOH stripper. 25 mL solutions of 5 mg/L, 50 mg/L and 500 mg/L phosphate were each individually equilibrated with 50 mg of LDHBC (at pH 7 and 25 °C) for 6 h. Solutions were then filtered and recovered. LDHBC was over dried at 80 °C for 2 h and equilibrated with 25 mL 1 M NaOH for 6 h at 25 °C (200 rpm). Contents were filtered and LDHBC was dried in an oven as above. This LDHBC was used in two more sorption-stripping cycles. Phosphate contents in the filtrates after each sorption/ stripping cycle was analyzed using UV-vis spectroscopy.



Scheme 2. Phosphate ion-exchange sorption mechanisms.

2.5.4. Fe/Mg leaching studies

Fe/Mg leaching tests employed 50 mg of LDHBC equilibrating in 25 mL solutions of DI water containing 10, 100, 500, 1500 and 2500 ppm of phosphate for 3 h. These solutions were filtered and the for Fe and Mg contents were determined using an inductively coupled plasma mass spectrophotometer (ICP-MS) (PerkinElmer SCIEX, ELAN DRC II).

2.5.5. Column study

LDHBC fixed-bed continuous flow adsorption studies were conducted, and breakthrough curves were constructed to assess their potential in scaled-up applications. Approximately 1 g of LDHBC (125-300 μm particles) was packed in a (diameter: ${\sim}3$ cm and bed length: ${\sim}14.5$ cm) plastic pipette (with a quartz wool exit) by transferring a warm aqueous solution to remove any air bubbles. Column was tapped with a rubber hose to ensure even packing. A 0.11 mL/min steady flow was maintained and a total of 1 L 60 mg/L phosphate solution was passed through column at 25 °C. Elute was collected at frequency of 30 min and examined for phosphate concentrations.

3. Results and discussion

3.1. Characterization of biochar

3.1.1. Surface area and elemental analysis

The Fe:Mg % weight ratios for both LDH and LDHBC were \sim 1:1, which confirms that the Fe:Mg mole ratios in LDH (0.19:0.39) and LDHBC (0.14:0.31) are close to 1:2 in the general $Mg_{1-0.33}^{2+}$ -Fe_{3-0.33}(OH)₂]^{0.33+}Cl^{0.33-}·nH₂O empirical formula in both preparations [30]. The amount of water (n) may vary depending on the LDH preparation method. Combustion elemental analyses of LDHBC (Table 1) show lower C content (53.1 wt%) versus BC (74.6%) due to the significant LDH weight contribution. The carbon (1.2%) found in LDH likely originates from small amounts of carbonates formed during the LDH precipitation.

The amount of O in LDHBC is very small compared to its BC precursor. The washings plus stirred exposure to 10% NaOH during LDH formation/precipitation may have further removed residues carboxylic acid, phenolic, and other acidic organic residuals from the BC [31]. The BC originated from fast pyrolysis at a residence time of 1–10 s at 900–1000 °C, which produces high surface areas (695 m²/g) and pore volumes (0.264 cm³/g). The high C/H (39.3)

ratio and observed O/C (0.28) ratio of BC result from pyrolytic loss of oxygen and hydrogen at high temperature. The neat LDH $\rm N_2$ BET surface area was only 14.3 $\rm m^2/g$, less than the (48.7 $\rm m^2/g)$ value reported in the literature [32]. Literature values were only available for the more crystalline calcined (120 °C for 24 h) Mg/Fe-LDH, leading to this higher surface area. Calcination during LDHBC preparation have been avoided as it could lead to BC decomposition and lower LDHBC yield, and high temperature processes are considered costly.

The N_2 BET specific surface area for LDHBC was 267 m²/g suggesting that the LDH impregnation filled biochar surface pores resulting in a ~62% reduction of its original surface area (from 695 to 267 m²/g) and ~67% of its pore volume (from 0.264 to 0.0879 cm³/g). Impregnation of Fe-Mg LDH on the BC surface and into some pores to form LDHBC causes partial pore blockage and block N_2 access into a fraction of the BC micropores and ultramicropores. Likewise, a loss of ~83% of surface area (from 450 to 79 m²/g) and ~81% of its pore volume (from 0.1056 to 0.0204 cm³/g) was observed in CO_2 adsorption.

The BC ash (2.1%) originates from stable sodium, potassium, magnesium, calcium, and iron oxides and carbonates. LDHBC had a high ash content (41.7%) because of impregnated LDH.

3.1.2. Surface morphology and texture

LDH has a dense, rocky exterior while BC and LDHBC have porous surfaces. A longitudinal-tangential section of the wood is observed on BC SEM micrograph (Fig. 1a). Thus, secondary xylem elements can be identified, including tangentially cut radial parenchyma (one cell wide -uniseriate) between longitudinally cut tracheids and possibly fibers. Fig. 1c shows a longitudinal cut of a fiber casquete. A transverse section of this casquete is visualized in the upper right section of the picture, which displays three fiber lumens. The shape of the LDH is distorted hexagonal or quasispherical (Fig. 1e). Upon deposition of LDH on to biochar, the shapes become more indefinite (Fig. 1f). The effect of the BC surface on the LDH nucleation and growth during precipitation compared to the aqueous phase is not known. Phosphate-laden LDH and P-laden LDHBC shows more aggregated LDH particles. Some BC micropores are blocked by the LDH deposition on/in its lumen.

LDH precipitation from solution onto BC to form LDHBC was confirmed by the presence of intense magnesium and iron EDX peaks (Fig. S1) and elemental maps (Fig. 2) (~8.5% Mg and ~5.9% Fe). They clearly show co-existing positions of iron, magnesium,

Table 1Elemental, proximate analysis and surface area data for adsorbents.

Sample	% C	% H	% N	% O ^a	% Ash	%Fe	% Mg	^b N ₂ BET surface area (m ² /g)	^b N ₂ pore volume (cm ³ / g)	°CO ₂ BET surface area (m ² /g)	°CO ₂ pore volume (cm ³ /g)	^b Pore diameter (N ₂) (Å)	°Pore diameter (CO ₂) (Å)
ВС	74.6	1.9	0.1	21	2.4	0.1	0.5	695.1	0.264	450.1	0.1056	14.5	9.4
LDH	1.2	2.7	0.1	25.8	70.3	10.9 ^d	9.5 ^d	14.3	0.0035	7.4	0.0038	9.8	20.4
LDHBC	46.7	1.5	1.2	4.1 ^f	41.7	7.9 ^e	7.5 ^e	267.3	0.0879	78.5	0.0204	13.2	10.4

- ^a Calculated by the difference (0% = 100 (C + H + N + ash).
- ^b From N₂ BET adsorption isotherms at 77 K.
- ^c From CO₂ BET adsorption isotherms at 273.
- d Fe/Mg molar ratio = 0.19:0.39.
- e Fe/Mg molar ratio = 0.14:0.31.
- f This value is calculated by the difference and may not reflect the actual "O" content due to the formation of higher molecular weight oxides during ashing.

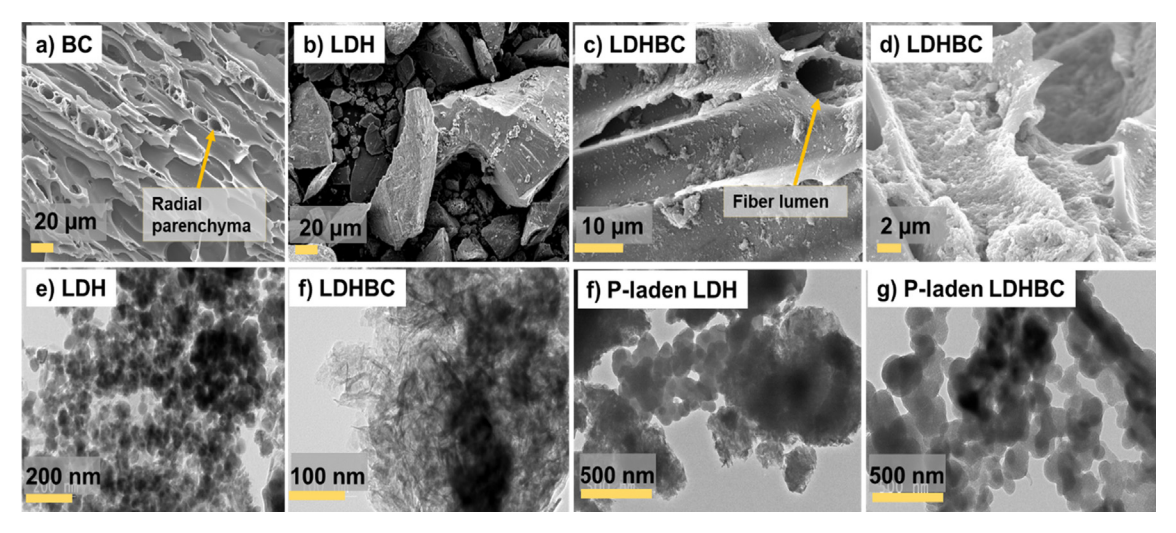


Fig. 1. (a-d) SEM micrographs BC, LDH, and LDHBC and (e-h) TEM micrographs of LDH, LDHBC, P-laden LDH and P-laden LDHBC.

and chlorine as evidence of LDH formation on BC. Chlorine disappeared upon phosphate sorption, providing evidence that ionexchange of chloride by phosphate occurs as LDH phases in LDHBC adsorb phosphate. TEM-EDS element maps (Fig. 3) show that phosphate is rather homogenously distributed over the LDH and LDHBC surfaces. LDH surfaces preferably adsorbed phosphate almost exclusively since the BC phase adsorb negligible phosphate [5] (Fig. S2) and the biochar LDHBC surfaces, where LDH was absent, contained < 0.05% P. TEM-EDS elemental mapping images (Fig. 3c and d) of the LDHBC upon P sorption showed significant amounts of P (brown dots) on the LDH surface (~7% in P-laden LDH and ~9% in P-laden LDHBC) (Fig. 3 c and d). These EDS analyses indicate LDH and LDHBC both have high phosphate adsorption capacities based on these high % P values (TEM detection limit ~0.5% wt.). The calculated P capacities calculated from these TEM-EDX mappings are ~70 mg/g (for LDH) and 90 mg/g (for LDHBC), which corresponds to ~ 215 mg/g and ~ 276 mg/g of phosphate (PO₄³⁻) adsorption on LDH and LDHBC. This approximation is based on the high wt. fraction of LDH in LDHBC and negligible phosphate adsorption on biochar phase, respectively. Typical iron/ magnesium-phosphate compounds are insoluble and form monolayer coatings on iron oxides precipitated onto biochars [33,34]. Apart from chemisorption, insoluble iron/magnesium-phosphate precipitates originating from the dissolution of Fe³⁺ and Mg²⁺, should be considered.

3.1.3. XRD analysis

The XRD patterns of LDH and LDHBC before and after phosphate adsorption are presented along with biochar in Fig. 4a. The broad peak at $2\theta = 22.7^{\circ}$ for biochar originates from the disfigured cellu-

lose crystal structure during high temperature pyrolysis [35]. Characteristic LDH diffraction planes ~11.2° (003), ~22° (006), ~34° (012), $\sim 37.9^{\circ}$ (015), $\sim 45.3^{\circ}$ (018), $\sim 59.2^{\circ}$ (110) and $\sim 60.3^{\circ}$ (113)were observed for pure LDH and LDHBC samples [36]. This confirms that Fe-Mg LDH was satisfactorily synthesized and effectively deposited onto the biochar in LDHBC. In addition, the peaks at 31.7° and (32.8°, 62.1° and 63.5°) in both LDH and P-laden LDH are attributed to small amounts of maghemite (Fe_2O_3 or γ - Fe_2O_3) and magnetite (Fe₃O₄), respectively, formed during the preparation of LDH [5,37]. The phosphate-loaded LDH and LDHBC displayed new peaks not observed prior to phosphate sorption, due to specific stoichiometric iron/magnesium phosphate compounds generated during phosphate uptake. The peak at ~26.5° in P-laden LDHBC is assigned to iron phosphates or NaFePO₄ [38]. The peaks at ~40.3° and ~49.2° correspond to FePO₄·2H₂O and FePO₄ [orthorhombic (JCPDS 33-667) and monoclinic (JCPDS 33-66)] [39,40] respectively. The ~53.8° peak represents Mg₃(PO₄)₂ (JCPDS 33-876) [38]. The P-laden samples were prepared using a solution of 1000 mg/L phosphate to observe significant changes in XRD. This may have triggered dissolution of some iron and magnesium from the LDH and subsequent formation and deposition of these stoichiometric compounds. Similar effects were observed in our previous work on phosphate and arsenate sorption onto magnetitedispersed BCs [5,41].

The LDH crystallite sizes were found using the Debye-Scherrer equation [42], $(D_{hkl} = 0.9\lambda/\beta\cos\theta)$ where λ is the wavelength used in the X-ray experiment (nm), β is the full-width at half-maximum (FWHM) value in radians for XRD diffraction lines and θ is one half of the 2θ diffraction angle. The crystallite sizes determined using the most intense XRD peak (003), were 9.4, 8.5, 18.1

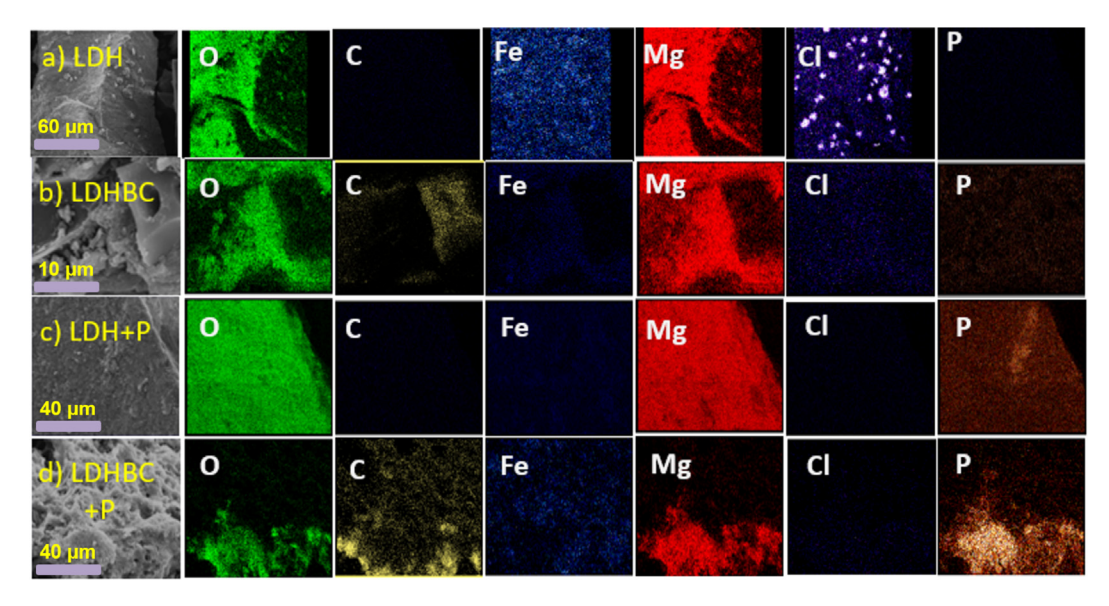


Fig. 2. SEM/EDS elemental maps for a) LDH, b) LDHBC, c) Phosphate-laden LDH (234.3 mg/g phosphate), and d) Phosphate-laden (1279.6 mg/g) LDHBC.

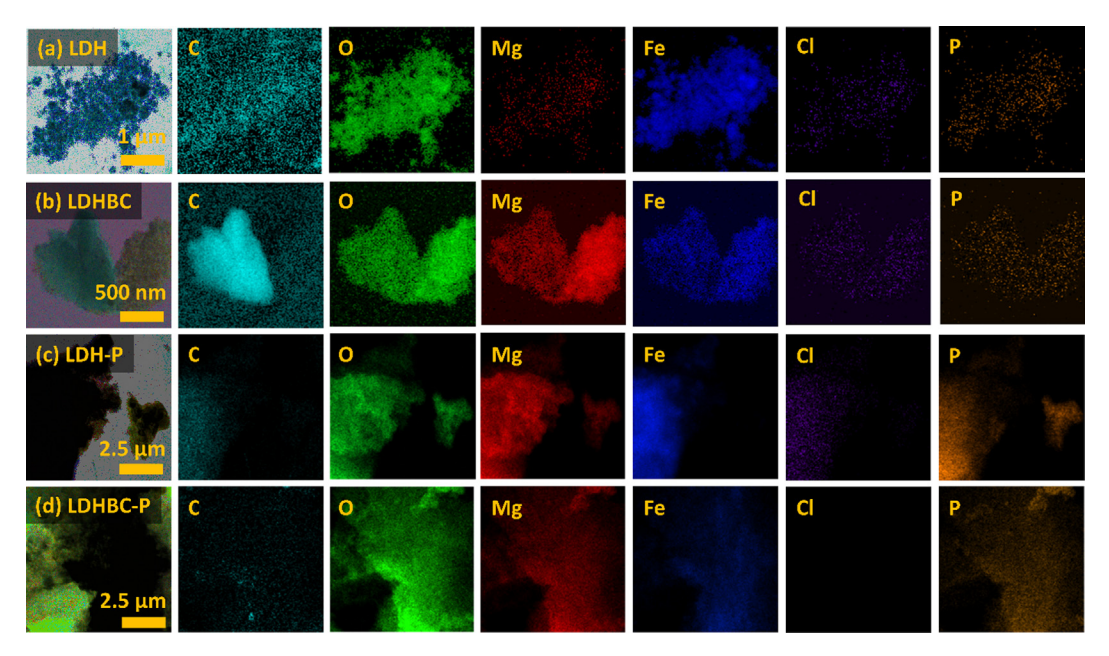


Fig. 3. TEM/EDS elemental maps for a) LDH, b) LDHBC, c) Phosphate-laden LDH (234.3 mg/g phosphate), and d) Phosphate-laden (1279.6 mg/g) LDHBC.

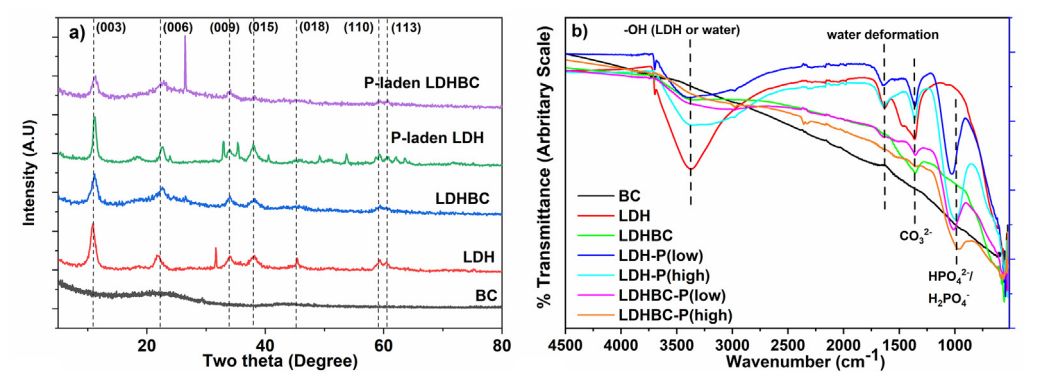


Fig. 4. a) Powder XRD and b) FT-IR data for LDH, LDHBC, P-laden LDH, and P-laden LDHBC.

and 10.1 nm for LDH, LDHBC, P-laden LDH and P-laden LDHBC respectively. P-laden LDH and LDHBC showed an increase in crystallite size, as the LDH interlayer distance expands upon phosphate sorption. Chemisorption of phosphates or stoichiometric magnesium or iron phosphate compound formation may complete.

The important XRD lattice parameters (a, c and c') and interlayer thickness of LDH were calculated using the equations below and in Table 2, assuming 3R polytipism (R3m space group) for the LDH [18]. The lattice parameters and inter-planar spacing (d_{hkl}) values were estimated using the Bragg equation [43], $(d_{hkl} = \lambda/2\sin\theta)$, where λ is the wavelength of X-ray (nm), θ is half of the diffraction angle, $a = 2d_{(110)}$ and $c = 3d_{(003)}$. Alternatively, "c" was calculated using $c = 3d_{003} + 6d_{006} + 9d_{009}/3)$] equation, to find interlayer distance [interlayer distance = c' - brucite-like sheet thickness (0.434 nm), where c'=c/3 [44]. The "a", "b", and "c" values determined for the LDH, LDHBC and their P-laden analogs are consistent with those reported in literature for Fe/Mg-LDH (a = 0. 308-0.311 nm and c = 0.308-0.311 nm) [18,45]. The selected area electron diffraction (SAED) pattern indicated concentric diffraction rings for all LDH-containing samples (Fig. S3) revealing their crystallinity and presence of pure LDH phases [46]. This unequivocally confirms the presence of LDH on BC and its stability during phosphate sorption from solutions concentrations from 2.5 to 1000 ppm. The ionic radius of Cl⁻ is 0.18 nm and for phosphate 0.24 nm. Thus, the interlayer d-spacing is expected to increase with phosphate sorption. However, this radius difference is small (~0.06 nm) to observe a significant interlayer spacing increase from phosphate sorption. Chemisorption and stoichiometric phosphate precipitation may also affect the accuracy of these calculations.

3.1.4. FTIR spectroscopy

Fig. 4b displays the FT-IR spectra for BC, LDH, LDHBC, P-laden LDH and P-laden LDHBC. The FTIR spectrum of BC does not give sharp bands, due to the lack of polar functionality or poor ATR transmission. Small amounts of several types of individual oxygenated groups do not produce strong bands. During the pyrolysis at 400 °C and above dehydration, decarboxylation, deamination etc. occur [47]. BC, precursor of LDHBC, was originally pyrolyzed at 900 °C, although for 1-10 secs. This lack many distinct bands is an advantage for analysis of the deposited LDH of LDHBC. The FT-IR of neat LDH exhibited bands at 3374 cm⁻¹ and the sharp peak at 1362 cm⁻¹ were assigned to -OH stretching and bending vibrations from the hydroxyl groups on the LDH layers and interlayer water molecules [18]. Specific resolved peak adsorptions in 900-400 cm⁻¹ range of the stretching and bending modes of Fe-O, Fe-O-Fe, Mg-O and Mg-O-Mg bonds are not observed [18]. Phosphate laden-LDH and LDHBC (at pH 7) show a strong peak at $\sim 971 \text{ cm}^{-1}$ corresponding to the v3 band vibrations of HPO₄²⁻ or $H_2PO_4^-$ (Fig. 4) which is absent in the neat adsorbents [48]. This confirms phosphate sorption took place. An increase of the intensity and shifts were observed within the (3409–3399 cm⁻¹) O—H stretching region upon exposing either LDH or LDHBC to increasing phosphate solution concentrations (from 1000 to 10000 mg/L) during adsorption. This could be due to the -OH contribution from adsorbed HPO₄ or HPO₄²⁻ ions. The peaks in the 1335 cm⁻¹ region were assigned to CO_3^{2-} [18]. The carbonate was introduced into the LDH as an impurity in the NaOH or from CO₂ uptake from air during LDH synthesis.

3.2. Batch sorption data

3.2.1. Effect of solution pH on phosphate adsorption

The LDH and LDHBC points of zero charges (PZCs) are \sim 10.6 and \sim 10.5, respectively. The PZC of BC is reported in our previous studies (\sim 9.2) [49]. The basic PZC value of BC is due to Na, K, Mg and Ca

carbonates and oxide/hydroxides formed during the pyrolysis process [16,49]. The LDH contains Mg^{2+} and Fe^{3+} in the sheets with hydroxy functions attached. The $Mg(OH)_2$, α -FeOOH, and δ -FeOOH PZCs are 12.3, 6.7, and 7.4 respectively. The LDH and LDHBC surfaces should then give a PZC between that of $Mg(OH)_2$ and that of FeOOH [50]. HO $^-$ surface adsorption and Cl^-/HO^- ion exchange may occur simultaneously during the PZC titration. In this experiment, the two processes have not been separated, so these PZC values are considered approximate.

The acid dissociation constants for H_3PO_4 are $pK_{a1}=2.12$, $pK_{a2}=7.21$, and $pK_{a3}=12.67$ (Fig. 5a). From pH 0 to 4.7, dominant phosphorous species are H_3PO_4 and $H_2PO_4^-$. $H_2PO_4^-$ and HPO_4^{2-} dominates in the pH 4.7–9.7 range. From pH 9.7–14 HPO_4^{2-} and PO_4^{3-} are the dominant species. The percentage of phosphate adsorbed onto both LDH and LDHBC was substantial and similar over the entire pH 1 to 13 range (Fig. 5a). A small sorption capacity drop was observed for both LDH and LDHBC after pH 11 due to electrostatic repulsion between the LDH surface and HPO_4^{2-} and PO_4^{3-} ions present from pH 11–13 and competition from HO_2^{3-} LDH materials are known to have a high anion exchange capacity, which dominates these interactions [51]. Adsorption is almost independent of solution pH.

3.2.2. Sorption kinetics

Phosphate removal on both LDH and LDHBC was plotted versus the equilibrium time (Fig. 5b) at 50, 100 and 500 mg/L initial concentrations. Both adsorbents (at pH 7, 25 °C with a 2 g/L dose) exhibited high initial phosphate adsorption rates. Equilibrium was attained after ~3 h for both adsorbents at all three concentrations. Experimental data gave reasonable (R² ~ 0.9) fits (Table 3) to the pseudo-second-order model (equation (5)). Due to the poor correlation coefficients and large uncertainty in fittings, both pseudo-first-order and Elovich models were disregarded.

$$\frac{t}{q_{t}} = \frac{1}{k_{2}q_{e}^{2}} + \frac{t}{q_{e}} \tag{5}$$

Here, t is contact time, q_e is the adsorbed concentration of phosphate (mg/g) at equilibrium, q_t is the equilibrium concentration of phosphate (mg/g) at time t, and k_2 is the rate constant.

3.2.3. Adsorption isotherms

The Langmuir [52] (Eq (6)) and Freundlich [53] (Eq (7)) models were used to describe the isotherm data (Fig. 5d–g and Table 3). Both models fit well, preventing distinguishing between monolayer or multilayer sorption. At pH 7, both $\rm H_2PO_4^-$ and $\rm HPO_4^{2-}$ species coexist (Fig. 5a) in solution and are the species that adsorb.

$$q_e = \frac{q_0 K_L C_e}{(1 + K_L C_e)} \tag{6} \label{eq:qe}$$

$$q_e = K_F C_e^{(1/n)} \tag{7}$$

Here, q_e is the amount of adsorbate on the adsorbent at equilibrium (mg/g), q_o is the theoretical isotherm saturation capacity (mg/g), C_e is the equilibrium concentration (mg/L), n is adsorption intensity, K_L is the Langmuir isotherm constant (L/mg) and K_F is the Freundlich isotherm constant.

At 25 °C, the Langmuir maximum capacities were ~234 and ~1278 mg/g for LDH and LDHBC, respectively. Phosphate removal was expected to increase in LDHBC versus LDH due to the excellent dispersion of LDH particles on the BC surface and due to the presence of iron oxide and magnesium oxide phases. Similar phenomena have been observed where previous studies compared the phosphate sorption onto LDH and LDHBC [54] and as well as in our work with phosphate sorption magnetite dispersed on BC [5]. The adsorption capacities of both LDH and LDHBC increased with

Table 2Powder XRD lattice parameters calculated for LDH, LDHBC and their P-laden analogues.

Sample	d ₀₀₃	d ₀₀₆	d ₀₀₉	с	c'	Interlayer distance (nm)	a (nm)	c (nm)
LDH	0.82	0.40	0.24	5.52	1.84	1.41	0.31	2.45
LDHBC	0.79	0.39	0.24	5.44	1.81	1.38	0.31	2.39
LDH-P	0.79	0.39	0.24	5.46	1.82	1.38	0.31	2.38
LDHBC-P	0.78	0.39	0.24	5.39	1.80	1.36	0.30	2.34

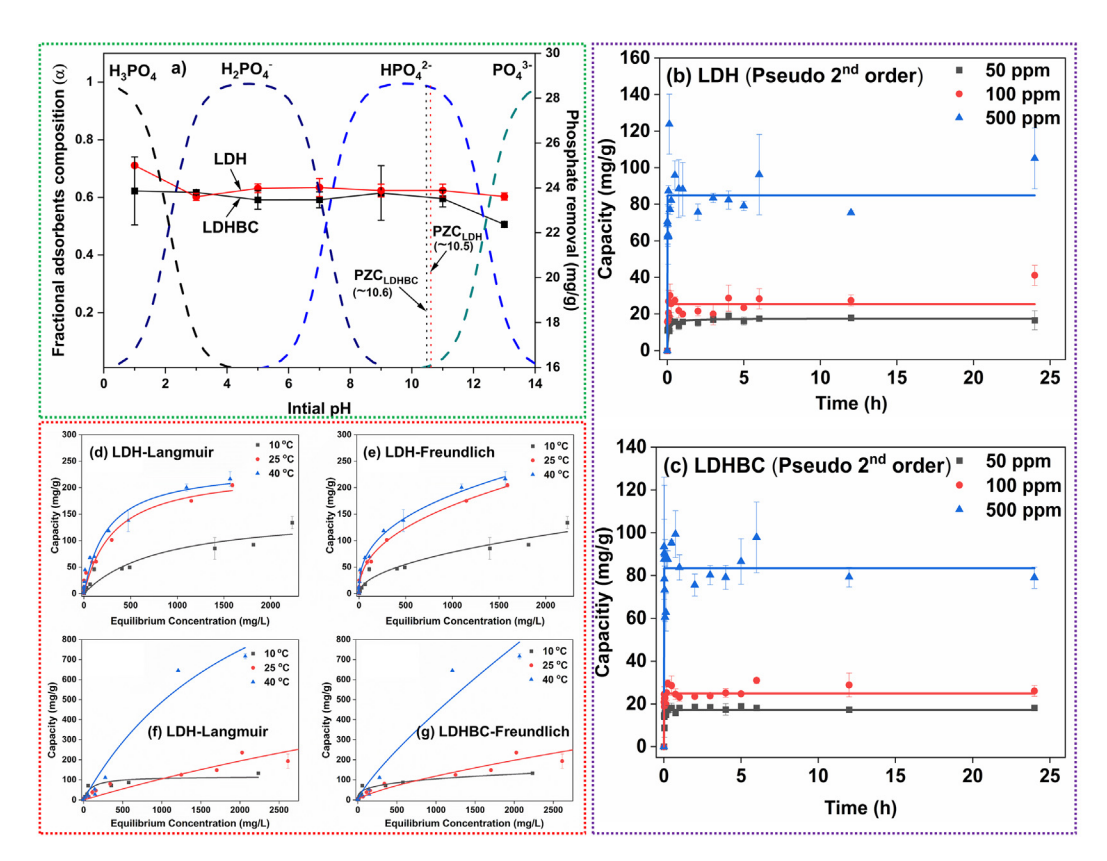


Fig. 5. a) pH dependence of phosphate adsorption onto LDH and LDHBC (at 25 °C and 6 h equilibration) and fractional composition curves for phosphate speciation. Pseudo 2nd order adsorption vs time model plots (at 25 °C and pH 7) for b) LDH and c) LDHBC at 0.05, 0.1 and 0.5 g/L initial concentrations. d), f) Langmuir and e), g) Freundlich isotherm fits of phosphate sorption (25 °C, pH = 7 and 6 h of equilibration) for LDH and LDHBC (Error bars represent the standard deviation of 3 replicates).

Table 3Pseudo 2nd order kinetic data for LDH and LDHBC^a, Langmuir and Freundlich isotherm model data for phosphate on LDH and LDHBC (25 °C, pH = 7 and 6 h equilibration)^b and Thermodynamic parameters for the net observed adsorption of phosphate by LDHBC from 10 to 40 °C.

Pseudo 2nd	order kinetics data	Isotherm data										
							Langmuir Is	otherm		Freun Isothe		
Adsorbent	Concentration (ppm)	R^2	k ₂	q _{cal} (mg/g)	q _{exp} (mg/g)	Temperature	q ₀ (mg/g)	K _L (L/mg)	R^2	K _f	n	R ²
LDH	50	0.996	0.72	17.51	16.57	10	154.2	0.0012	0.99	2.4	2.0	0.99
	100	0.914	1202.63	25.25	41.09	25	234.3	0.0031	0.99	8.8	2.3	0.99
	500	0.948	7607.36	84.91	105.04	40	240.5	0.004	0.99	13.6	2.6	0.99
LDHBC	50	0.97	1318.3	17.19	18.19	10	117.2	0.0105	0.99	13.7	3.4	0.99
	100	0.969	2266.33	24.87	26.09	25	1279.6	8.95E-05	0.99	0.8	1.4	0.99
	500	0.971	699.09	83.37	79.03	40	1588.9	0.0004	0.99	1.6	1.2	0.99
Vant' Hoff d	ata for LDHBC											
	T (°C)	\mathbb{R}^2	K _{ads}	lnK _{ads}	ΔG^0 (kJ/mol)	ΔH ⁰ (kJ/mol)	ΔS ⁰ (kJ/mol·K)					
Langmuir	10	0.99	1.20E+03	7.09	-0.6	•	0.16					
-	25		3.10E+03	8.04	-1.7	29.75						
	40		4.00E+03	8.29	-2.8							

^a Significant figures of the rate constants and regression coefficients are based on the model fittings and may not reflect the actual uncertainties of experimental data.

^b Isotherm capacity data were generated by local refinement of empirical isotherm equations via the Levenberg–Marquardt distant nonlinear regression algorithm in Origin2019 using the average value of 3 replicates for each data point. Significant figures on isotherm specific capacities and regression coefficients are based on the model fittings and may not reflect the actual uncertainties of experimental data.

rising temperature, confirming endothermic phosphate uptake, which is consistent with previous reports [55].

The capacity (q_0) increases for both adsorbents (Table 3) as temperature rises from 10 °C to 25 °C, but that observed going from 25 °C to 40 °C for LDHBC (1280 to 1589 mg/g) is surprising. Several factors may contribute to high capacities at 25 °C and 40 °C (1) Maximum Langmuir capacities solely depend on model fittings, which may be less certain at 40 °C and higher initial phosphate concentrations (>500 ppm), (2) Equilibrium may only be partially achieved as more diffusion into small BC pores occurs accessing more LDH. Greater filling of the available LDH interlayers via ion-exchange would also lead to greater phosphate uptake, (3) High temperatures and higher initial phosphate concentrations may induce phosphate chemisorption/stoichiometric reactions (Fe-O-P and Mg-O-P and perhaps other bond forming) on the surface or other phases. As temperature and concentration increases, such reactions can be more favored when suitable surface sites are reached by diffusion. Given the phase complexity hybrid system, this is a distinct possibility. This includes the BC and LDH surfaces, the LDH interlayers and any Mg/Fe oxides that might have deposited from side reactions during the LDH precipitation. Additionally, this Mg/Fe-LDH and other potential iron oxides and salts present might undergo Fe^{2+/3+} or Mg²⁺ leaching into phosphate solutions especially as temperature or phosphate concentration rises. As these ions become available, they will react to form insoluble iron phosphate [(Fe₃(- PO_4 ₂, $FeHPO_4$, $Fe(H_2PO_4)_2$, $FePO_4$, $Fe_2(HPO_4)_3$ and $Fe(H_2PO_4)_3$] or the magnesium phosphate species [Mg₃(PO₄)₂, MgHPO₄ and Mg (H₂PO₄)₂] which then precipitate on adsorbent surfaces. The Fe/ Mg dissolution data (Fig. S4) indicates that when going from 25 °C to 40 °C, the dissolution of Fe/Mg increases. Also, when increasing the initial phosphate concentration, ion leaching has increased and may lead to more stoichiometric compound precipitation. However, it is not experimentally possible to find the total concentrations of the ions leached as they can precipitate out immediately with phosphate in the solution.

Adsorbate-triggered iron dissolution followed by precipitation of insoluble salts was observed on both phosphate and arsenate sorption onto Fe_2O_3 /biochar hybrid adsorbents [5,41]. Finally, higher temperature could drive occlusion via aggregation on the LDH and iron/magnesium oxide covered adsorbent surface. All in all, the high adsorption capacities at both 25 °C (at higher concentrations) and 40 °C should be considered real, but approximate.

3.2.4. Thermodynamics of adsorption

The Gibbs free energy (ΔG), enthalpy (ΔH) and entropy (ΔS) changes were calculated using van't Hoff's equations. First, the Langmuir isotherm constant (K_L) for each temperature was transformed to dimensionless constants (K_{ads}) via multiplying by the density of the liquid phase ($\sim 10E06$ mg/L) [56]. The negative ΔG values (Table 3) indicated a spontaneous adsorption, and their magnitudes increased with temperature. However, if more than one process is responsible for phosphate removal, the ΔG , ΔH and ΔS terms will not be specific for the single ion exchange process of phosphate for chloride in the LDH.

The positive Δ H (29.8 kJ/mol) confirmed an endothermic phosphate overall removal process occurred. Physisorptions occur when Δ H < 20 kJ/mol and chemisorptions occur when Δ H > 40 kJ/mol [57]. Δ H \sim 30 kJ/mol suggests that phosphate adsorption on LDHBC is a physisorption process but it may represent the sum of more than one process occurring. This dehydration process is endothermic and may exceed the energy release by the ions to be attached to the adsorbent surface, thus resulting in an overall endothermic process [55]. The positive value of Δ S° showed randomness slightly increased during phosphate uptake onto LDH. The release of water molecules and Cl $^-$ from the interlayer and loss of water of hydration from phosphate species contribute to an overall entropy increase

relative to confinement of phosphates and differences in the new hydration of Cl⁻ and released water. Other factors like increased randomness at the sold-liquid interface might contribute reflecting extra translational entropy gained by water [55].

3.3. Assessment of the suitability for applied eutrophic water treatment

3.3.1. Ion competition

Challenges associated with treating eutrophic water by adsorption will be linked to the existence of competing ions. LDHBC is a multiphase adsorbent with three or possibly four phases (*i.e.*, carbonaceous biochar, mineral phase in biochar, LDH, and Fe/Mg oxides) that can interact with different ions. Thus, significant understanding is required for applied water treatment adsorbent design. Fig. 6a displays the effects of nine individually competing ions, at 0.01, 0.1 and 1 mM concentrations and 25 °C. Here LDHBC removes aqueous phosphate present at 50 mg/L. In the absence of competing anions, LDHBC's phosphate sorption capacity was ~8.5 mg/g.

The presence of some ions raises while other ions lower LDHBĆs sorption of phosphate. MoO_4^{2-} , for example, enhances phosphate uptake by LDHBC. This may be due to the increased ionic strength of the solution. Carbonate, arsenate and selenate decreased LDHBĆs phosphate uptake at 0.1 and 1 M but not at 0.01 mM. This competition increased as their concentration rose from 0.1 to 1 M. Nitrate, dichromate, chloride, fluoride and sulfate caused negligible competition with phosphate sorption.

The anion-exchange capacity of LDHs is governed by the degree of H-bonding and Coulombic interactions of the interclated anions in pristine LDH or LDH on LDHBC. H-bonding is a more crititical factor in exchange reactions of PO₄³⁻, whereas Coulombic interactions dominate in Cl⁻ intercalated LDHs. The interaction magnitudes depends on the speciation and anion orientation, with a crystal chemical basis [51]. Arsenate is a tetrahedral ion similar to phosphate and their respective sizes are ~248 pm and ~238 pm. One might expect them to have similar affinities to the LDH interlayer. The carbonate ion is smaller (~178 pm) which could strengthen competitive inhibition of phosphate uptake verses arsenate. However, its trigonal planar structure might lead to a lower affinity versus arsenate.

How the presence of all nine competing ions together, at three different concentrations, influenced the removal of 50 mg/L aqueous phosphate solution by LDHBC is also presented in Fig. 6a. The presence of nine ions at 0.01 mM slightly increased the phosphate sorption. This may result from the increased solution ionic strength. However, increasing the concentration of all nine ions (from 0.01 to 1 mM), which significantly raised the ionic strength, did not increase in phosphate sorption, but rather sharply decreased it due to the high cumulative competitive effects.

Phosphate removal in the presence of nine ions, at 1 mM each, decreased to ~12.5% of that adsorbed when all nine were present at 0.01 mM. The influence over phosphate uptake in the presence of the ion mixture were significant compared to their individual effect. LDHBC exposes four phases in adsorption, its LDH phase, iron/magnesium oxide particles, carbonaceous BC and BC's mineral surfaces. All may exhibit different electrostatic interactions and other adsorptive attractions with competitive ions and phosphate. The competitive enthalpic and entropic effects of anions in water should also be considered when designing a phosphate treatment system.

3.3.2. Application of LDHBC in environmental water samples

The remediation performance of LDHBC in a eutrophic system was investigated using a sample of lake water and pond water

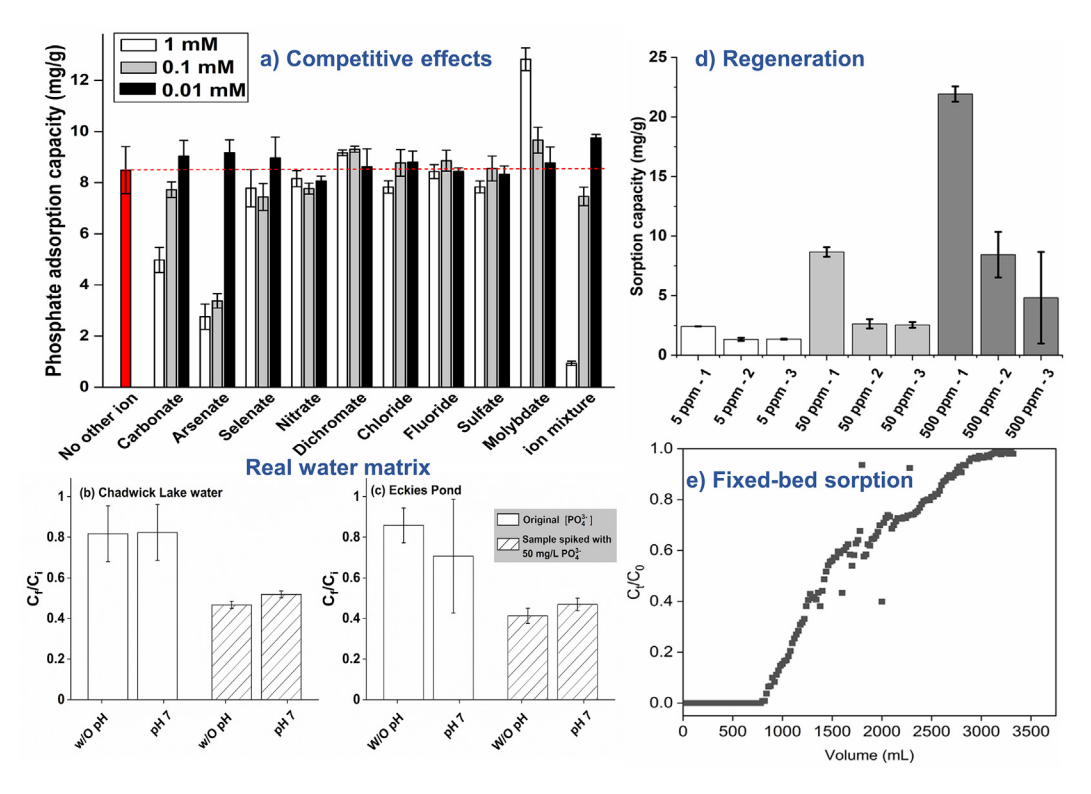


Fig. 6. a) Effect of nine individually competing ions and their mixtures, at three different concentrations (0.01, 0.1 and 1 mM) on the removal of 50 mg/L aqueous phosphate solution for LDHBC (50.0 mg dose of adsorbent, 25 °C, 200 rpm agitation and 6 h equilibration). For the sake of comparison, a red dotted line is traced based on the control 'no other ion' treatment, Comparison of phosphate adsorption from b) lake water and c) pond water, under various conditions (from the original samples, the pH 7 and after adjusted solutions, 50 mg/L phosphate spiked solutions (pH 7.2 and 7.3) and 50 mg/L phosphate solutions (pH 7.2 and 7.3) and after adjusting to pH 7) at 25 °C (LDHBC concentration of 0.2 g/L, 200 rpm and 6 h equilibrium time, d) sorption capacities for three sorption regeneration cycles carried out on LDHBC samples which adsorbed phosphate at 5, 50 and 500 mg/L initial aqueous concentrations and then stripped this adsorbed phosphate with 1 M NaOH. Error bars are the standard deviation for three repetitions. *The stripping capacities or percentages were not shown here because they were ~100% for all cases and e) fixed-bed phosphate sorption breakthrough curve onto LDHBC where Ct is the effluent concentration at the time t and C_0 is the initial effluent concentration. (For interpretation of the references to colour in this figure legend, the reader is referred to the web version of this article.)

(Fig. 6b and c). The initial pH and phosphate concentrations were (8.6 and 9.3) and (0.20 \pm 0.02 and 0.22 \pm 0.03 mg/L), respectively. The lake and pond water pHs were adjusted to pH 7 and batch phosphate sorption was studied under both initial and adjusted pH conditions. The sorption capacities were 0.08 \pm 0.01 mg/g and 0.10 \pm 0.01 mg/g for lake and pond waters at their original pH. The pH 7 adjusted solutions also showed similar sorption capacities of 0.08 \pm 0.01 and 0.08 \pm 0.03 mg/g, respectively. Complete sorption could not be achieved due to interfering ions present in the solutions and slow kinetics at the low phosphate concentrations (0.20–0.22 mg/L) present.

These experiments were repeated by spiking phosphate ions to bring final phosphate concentrations to 50 mg/L [1) Without adjusting pH (lake water pH = 7.2 and pond water pH = 7.3) and 2) adjusting both to pH 7]. In either case, the capacity change was small. Lake water and pond water at their original pH gave capacities of 11.7 ± 0.4 and 10.3 ± 0.9 mg/g, respectively. The pH 7 solutions provided 13.0 ± 0.4 and 11.7 ± 0.8 capacities, respectively. For a better comparison, phosphate solutions were prepared in de-ionized water at pH 7, 8.6 and 9.3 and gave capacities of 9.4 ± 0.5 , 8.6 ± 0.1 and 7.6 ± 0.6 mg/g respectively. The lake water matrix is complex verses DI water. The slight increase adsorption capacity for lake and pond waters could be ionic strength enhancement by co-existing ions [58].

3.3.3. Regeneration study

LDHBC sorption-regeneration were studied using a 1 M NaOH stripper (Fig. 6d) at 5, 50 and 500 mg/L initial phosphate concentrations to load LDHBC. NaOH can strip phosphate due to highly competitive effects from smaller size (~110 pm) compared to phos-

phate (\sim 238 pm). LDHBC's phosphate capacities during the first sorption cycles were 2.42, 8.7 and 21.9 mg/g from 5, 50 and 500 mg/L aqueous concentrations, respectively. LDHBC's Langmuir phosphate sorption capacity at 25 °C is 1279.6 mg/g. Regenerations may be more challenging when the maximum capacity is not fully reached. The first adsorbent/stripper contact occurs at sites where interactions are strong and therefore do not allow stripping agents to influence competitive interactions.

When 1 M NaOH was used to strip phosphate-laden LDHBC, after it had sorbed phosphate from solution of all three concentrations, almost 100% of phosphate was stripped. However, after the 1st regeneration of the LDHBC sample from the 5 ppm phosphate solution, the phosphate uptake is reduced to ~50% in both 2nd and 3rd cycles (Fig. 6d). Higher concentrations (50 and 500 ppm) phosphate-laden LDHBC showed higher capacity drops (~28% in both cycles for 50 ppm and ~38% and ~22% for 500 ppm). Proton removal from LDHBC by hydroxide at LDHBC surface sites may have created a high negative charge density on the surface, which led to strong electrostatic repulsions and desorption of the phosphate ions. In addition, the hydroxide ion could accumulate in the LDH interlayer structure. This would reduce H-bonding to phosphate and hydrogen phosphate anions and raise electrostatic repulsions, leading to phosphate stripping.

There are two significant applications of the findings in this experiment. First, LDHBC can be used to adsorb moderate to dilute phosphate concentrations (<5 ppm). Secondly, they can be used to amend nutrient depleted soil as a slow-release phosphate fertilizer. The slow release of phosphate in the fertilizer reduces the phosphate runoff in irrigation systems.

Table 4Comparison of Phosphate Adsorption Capacities.

Adsorbent	temp (°C)	Equilibrium time	pН	BET surface area (m ² /g)	adsorption capacity (mg/g)	Ref.
MgO/BC nanocomposite from sugar beet tailings	22	24 h		70.0	835.0	[59]
Marine macroalgae BC	20	48 h		2.4	3.3	[60]
Waste-derived fungal biomass magnetite BC	25	24 h		53.0	23.9	[61]
BC/Mg/Al-assembled nanocomposites	10	24 h	6	14.1	335.0	[62]
	20				480.0	
	30				727.0	
2:1 Mg/Al-LDHs sugar cane leaf BC composite	25	1 h	3	10.17	53.4	[63]
3:1 Mg/Al-LDHs sugar cane leaf BC composite				11.41	72.1	
4:1 Mg/Al-LDHs sugar cane leaf BC composite				12.25	81.8	
MBC	25	2 min	3	312.6	91.3	[5]
	35				91.0	
	45				90.0	
Zn-Al LDH	25	72 h			35.9	[64]
	30				58.2	
	40				79.1	
	50				92.6	
Fe ₃ O ₄ Zn/Al-LDH	25	1 h		133	36.9	[65]
Fe ₃ O ₄ Mg/Al-LDH	25			71.9	31.7	
Fe ₃ O ₄ Ni/Al-LDH	25			50.9	26.5	
Mg/Mn Layered double hydroxides	10	3 d			6.2	[66]
	25				7.3	
	40				7.5	
Magnetite based nanoparticles	24		3	31	5.2	[34]
LDHBC	10	5 h	7		117.2	This study
	25				1279.6	
	40				1588.9	

3.3.4. Fixed-bed column sorption

Continuous flow fixed-bed experiments are important for scale-up design to predict breakthrough capacities, exhaustion capacities and regeneration requirements. LDHBC's fixed-bed performance was described using a breakthrough curve (Fig. 6d). The breakpoint time is reached, and the bed is judged to be ineffective when the concentration ratio C/C_0 [where C is the phosphate concentration at time t and C_0 is the initial phosphate (60 mg/L) concentration] reaches 1.0 rapidly. The breakthrough curve shape and mass transfer zone width depend on the influent flow rate, fixed-bed particle sizes, mass-transfer rate to the particles and pore diffusion, adsorption isotherm, etc.

The breakthrough and exhaustion capacities for LDHBC from mass balance were $\sim\!49.2~mg/g$ and $\sim\!100~mg/g$ respectively. Although significantly lower than batch adsorption (117 to 1202.63 mg/g), this material shows a potential for fixed-bed sorption or treating run offs. More experiments are needed to optimize the conditions to achieve a high breakthrough capacity.

3.3.5. Comparison of phosphate adsorption capacities

The exceptional sorption capacities achieved for LDHBC exceed or are comparable with adsorbents reported in the literature (Table 4). Examples are given (Table 4) for stoichiometric uptake (not true adsorption cases) by the formation of insoluble phosphates (MgO/BC and BC/Mg/Al). Due to this exceptional rapid uptake rates and low potential cost of LDHBC, this adsorbent is very promising and qualifies as a phosphate sequester.

4. XPS studies and proposed phosphate adsorption mechanism

The Low Resolution (LR) survey XPS data for BC, LDH, LDHBC, Pladen LDH and P-laden LDHBC are given Fig. S5 and Table S1. Only C1s and O1s peaks appear for BC. Mg1s, Fe2p and Cl2p XPS peaks occur in LDH. LDHBC also exhibits the presence of Mg, Fe and Cl due to the LDH deposited on LDHBC. LDHBC's C1s, O1s, Mg1s and Fe2p binding energies (BE) match with those of LDH, further confirming the deposition of Fe/Mg-LDH on BC surface. After phosphate sorption, P2p peaks appear for both LDH and LDHBC with

atomic % of 9.08 and 4.95%, respectively, while chloride XPS peaks disappear in both LDH and LDHBC in agreement with an ion exchange mechanism.

The High Resolution (HR) XPS spectra for BC, LDH, LDHBC, Pladen LDH and P-laden LDHBC are given Fig. 7 and data in Table S2. The C1s high resolution spectra were deconvoluted to CO_3^{2-} (289.27–289.85 eV), COOH(R) (287.06–299.65 eV), >C=O (285.85-287.76 eV), C-O (284.9-285.87 eV) and C-C, C=C and C-H (283.79-284.54 eV). O1s HR spectra was deconvoluted to Na auger/adsorbed water (534.1–536.38 eV), $CO_3^{2-}/-COOH(R)$ (533,24-533.88 eV), >C=O (532,26-532.81 eV), C=OH/P=OH/ M-OH (531.51-531.7 eV), M-O/P=O (530.33-531.08 eV) and Mg-O-Mg/Fe-O-Mg/Fe-O-Fe (529.57-529.93 eV) [67]. The Mg1s spectra comprise Mg-0 (1304.92–1306.07 eV), Mg(OH)₂/ Mg-O-P (1304.2-1304.89 eV) and Mg-O-Fe (1303.33-1303.81 eV). P2p was resolved to its H₃PO₄ analogue (134.35 eV) and M-O-P (133.72-133.88 eV) [67]. An example Fe2p deconvolution and peak assignment [5,68] is given in supporting material (Fig. S6).

Phosphate uptake on LDHBC occurs through ion-exchange (Scheme 2), and surface precipitation (chemisorption) plus stoichiometric compound formations (Section 3.2.3) all are possible. Most LDH phosphate adsorption occurs due to ion exchange mechanisms. Significantly, only weak bonding occurs between LDH interlayer anions or atoms with its octahedral sheets [22]. Ion-exchange occurs by displacing Cl $^-$ ions. Depending on the speciation $\rm H_2PO_4^-$, $\rm HPO_4^2^-$ or $\rm PO_3^4^-$, the amount of Cl $^-$ ion displaced may vary. This type of ion exchange was reported earlier with the exchange of sulfate ions with phosphate ions [63]. Inner sphere monodentate and bidentate surface complex formation is another type of phosphate adsorption mechanism involving the removal of water molecules or hydroxyl ions.

5. Conclusion

Fe/Mg-LDH dispersed on commercial Douglas fir biochar (LDHBC), prepared by a simple co-precipitation method, gave superior phosphate sorption capacities (1279.6 mg/g) versus bare

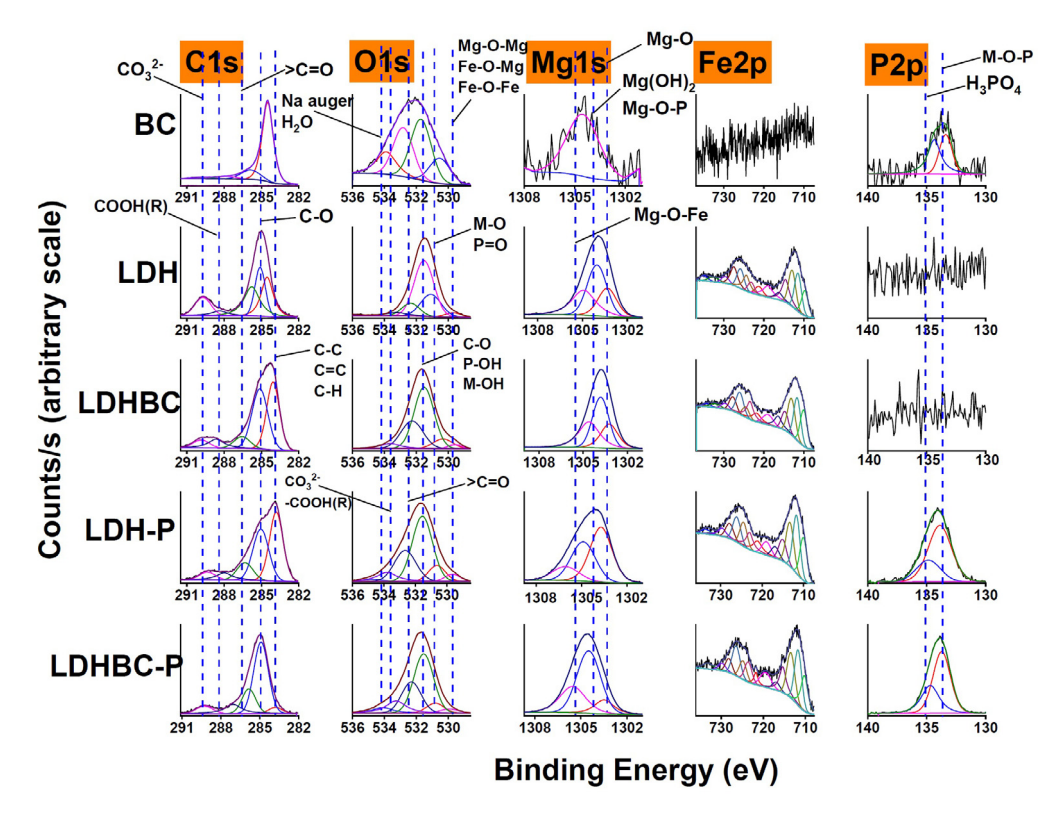


Fig. 7. High Resolution (HR) XPS spectra of C1s, O1s, Mg1s, Fe2p and P2p for BC, LDH, LDHBC, phosphate-laden LDH and phosphate-laden LDHBC *Due to the complex nature of (HR) XPS Fe2p spectra, these peaks are not assigned here and assignment is available in the supporting material.

LDH (243.3 mg/g) at 25 °C. Sorption was robust (pH independent, little interference from competitive ions, complex water matrix phosphate removal capability, potential cyclic sorption-stripping performance for low concentrations (≤5 ppm), and ability to treat low to moderate concentrations). Equilibrium was attained in < 5 h. Ion-exchange was the main sorption mechanism at lower concentrations (10-500 ppm), which was investigated by XRD, EDS and LR and HR XPS data. Chemisorption and stoichiometric phosphate compound formation were also considered at higher concentrations (>500 ppm) and 40 °C temperature. Also, upon impregnation of LDH, the biochar phase still retains a significant portion of its original portion surface area (~267 m²/g of its original ~695 m²/g) for adsorbing other contaminants during applied water treatment. This work advances the state of the art for environmentally friendly phosphate reclamation. Importantly, dispersion enhanced the LDH phase's adsorption of phosphate by ~6 times versus pure LDH particles. These phosphateladen adsorbents have potential to be used as a slow-release fertilizer.

CRediT authorship contribution statement

Sharifur Rahman: Conceptualization, Methodology, Investigation, Writing - original draft. Chanaka M. Navarathna: Conceptualization, Methodology, Investigation, Writing - original draft. Naba Krishna Das: Investigation. Jacinta Alchouron: Investigation. Parker Reneau: Investigation. Sean Stokes: Resources. Rooban V.K.G. Thirumalai: Formal analysis. Felio Perez: Formal analysis. E. Barbary Hassan: Formal analysis. Dinesh Mohan: Conceptualization, Visualization. Charles U. Pittman: Conceptualization, Supervision, Writing - review & editing. Todd Misna: Conceptualization, Supervision, Writing - review & editing, Funding acquisition.

Declaration of Competing Interest

The authors declare that they have no known competing financial interests or personal relationships that could have appeared to influence the work reported in this paper.

Acknowledgement

This work is supported by the National Science Foundation under NSF-INFEWS REU: Food, Energy, and Water Security, Grant (number 1659830).

Appendix A. Supplementary material

Supplementary data to this article can be found online at https://doi.org/10.1016/j.jcis.2021.03.114.

References

- N. Bektaş, H. Akbulut, H. Inan, A. Dimoglo, Removal of phosphate from aqueous solutions by electro-coagulation, J. Hazard. Mater. 106 (2-3) (2004) 101-105.
- [2] L.A. Lawton, G. Codd, Cyanobacterial (blue-green algal) toxins and their significance in UK and European waters, Water Environ. J. 5 (4) (1991) 460– 465
- [3] N.S. Palmstrom, R.E. Carlson, G.D. Cooke, Potential links between eutrophication and the formation of carcinogens in drinking water, Lake Reservoir Manage. 4 (2) (1988) 1–15.
- [4] N.N. Rabalais, R.E. Turner, B.K.S. Gupta, E. Platon, M.L. Parsons, Sediments tell the history of eutrophication and hypoxia in the northern Gulf of Mexico, Ecol. Appl. 17 (sp5) (2007) S129–S143.
- [5] A.G. Karunanayake, C.M. Navarathna, S.R. Gunatilake, M. Crowley, R. Anderson, D. Mohan, F. Perez, C.U. Pittman Jr, T. Mlsna, Fe3O4 nanoparticles dispersed on Douglas fir biochar for phosphate sorption, ACS Appl. Nano Mater. 2 (6) (2019) 3467–3479
- [6] K. Harrington-Hughes, Great Lakes water quality: a progress report, J. (Water Pollut. Control Federat.) (1978) 1886–1888.

- [7] A. Shalaby, E. Nassef, A. Mubark, M. Hussein, Phosphate removal from wastewater by electrocoagulation using aluminium electrodes, Am. J. Environ. Eng. Sci. 1 (5) (2014) 90–98.
- [8] T. Clark, T. Stephenson, P. Pearce, Phosphorus removal by chemical precipitation in a biological aerated filter, Water Res. 31 (10) (1997) 2557– 2563.
- [9] D. Zhao, A.K. Sengupta, Ultimate removal of phosphate from wastewater using a new class of polymeric ion exchangers, Water Res. 32 (5) (1998) 1613–1625.
- [10] C. Xuechu, K. Hainan, W. Deyi, W. Xinze, L. Yongyong, Phosphate removal and recovery through crystallization of hydroxyapatite using xonotlite as seed crystal, J. Environ. Sci. 21 (5) (2009) 575–580.
- [11] Y. Seida, Y. Nakano, Y. Nakamura, Rapid removal of dilute lead from water by pyroaurite-like compound, Water Res. 35 (10) (2001) 2341–2346.
- [12] K. Karageorgiou, M. Paschalis, G.N. Anastassakis, Removal of phosphate species from solution by adsorption onto calcite used as natural adsorbent, J. Hazard. Mater. 139 (3) (2007) 447–452.
- [13] M. Özacar, Adsorption of phosphate from aqueous solution onto alunite, Chemosphere 51 (4) (2003) 321–327.
- [14] W. Huang, S. Wang, Z. Zhu, L. Li, X. Yao, V. Rudolph, F. Haghseresht, Phosphate removal from wastewater using red mud, J. Hazard. Mater. 158 (1) (2008) 35–42.
- [15] K. Cheung, T. Venkitachalam, Improving phosphate removal of sand infiltration system using alkaline fly ash, Chemosphere 41 (1–2) (2000) 243–249.
- [16] Y. Yao, B. Gao, M. Inyang, A.R. Zimmerman, X. Cao, P. Pullammanappallil, L. Yang, Removal of phosphate from aqueous solution by biochar derived from anaerobically digested sugar beet tailings, J. Hazard. Mater. 190 (1–3) (2011) 501–507.
- [17] D. Bhargava, S. Sheldarkar, Use of TNSAC in phosphate adsorption studies and relationships. Effects of adsorption operating variables and related relationships, Water Res. 27 (2) (1993) 313–324.
- [18] R. Elmoubarki, F.Z. Mahjoubi, A. Elhalil, H. Tounsadi, M. Abdennouri, M.H. Sadiq, S. Qourzal, A. Zouhri, N. Barka, Ni/Fe and Mg/Fe layered double hydroxides and their calcined derivatives: preparation, characterization and application on textile dyes removal, J. Mater. Res. Technol. 6 (3) (2017) 271–283.
- [19] S.F. Almojil, M.A. Othman, Screening different divalent and trivalent metals containing binary and ternary layered double hydroxides for optimum phosphate uptake, Sci. Rep. 9 (1) (2019) 1–8.
- [20] X. Shi, C. Wang, J. Zhang, L. Guo, J. Lin, D. Pan, J. Zhou, J. Fan, T. Ding, Z. Guo, Zwitterionic glycine modified Fe/Mg-layered double hydroxides for highly selective and efficient removal of oxyanions from polluted water, J. Mater. Sci. Technol. (2020).
- [21] P. Li, P. Chen, Z. Liu, S. Nie, X. Wang, G. Wang, W. Zhang, H. Chen, L. Wang, Highly efficient elimination of uranium from wastewater with facilely synthesized Mg-Fe layered double hydroxides: optimum preparation conditions and adsorption kinetics, Ann. Nucl. Energy 107140 (2019).
- [22] G. Mishra, B. Dash, S. Pandey, Layered double hydroxides: a brief review from fundamentals to application as evolving biomaterials, Appl. Clay Sci. 153 (2018) 172–186.
- [23] D. Mohan, A. Sarswat, Y.S. Ok, C.U. Pittman Jr, Organic and inorganic contaminants removal from water with biochar, a renewable, low cost and sustainable adsorbent—a critical review, Bioresour. Technol. 160 (2014) 191– 202.
- [24] M. Inyang, B. Gao, Y. Yao, Y. Xue, A.R. Zimmerman, P. Pullammanappallil, X. Cao, Removal of heavy metals from aqueous solution by biochars derived from anaerobically digested biomass, Bioresour. Technol. 110 (2012) 50–56.
- [25] M. Uchimiya, L.H. Wartelle, V.M. Boddu, Sorption of triazine and organophosphorus pesticides on soil and biochar, J. Agric. Food. Chem. 60 (12) (2012) 2989–2997.
- [26] A. Solanki, T.H. Boyer, Pharmaceutical removal in synthetic human urine using biochar, Environ. Sci. Water Res. Technol. 3 (3) (2017) 553–565.
- [27] R. Li, J.J. Wang, L.A. Gaston, B. Zhou, M. Li, R. Xiao, Q. Wang, Z. Zhang, H. Huang, W. Liang, An overview of carbothermal synthesis of metal-biochar composites for the removal of oxyanion contaminants from aqueous solution, Carbon 129 (2018) 674–687.
- [28] P. Nautiyal, K. Subramanian, M. Dastidar, Adsorptive removal of dye using biochar derived from residual algae after in-situ transesterification: alternate use of waste of biodiesel industry, J. Environ. Manage. 182 (2016) 187–197.
- [29] D. Lozano-Calero, P. Martin-Palomeque, S. Madueño-Loriguillo, Determination of phosphorus in cola drinks, J. Chem. Educ. 73 (12) (1996) 1173.
- [30] S. Ashekuzzaman, J.-Q. Jiang, Strategic phosphate removal/recovery by a reusable Mg-Fe-Cl layered double hydroxide, Process Saf. Environ. Prot. 107 (2017) 454-462
- [31] A.G. Karunanayake, O.A. Todd, M.L. Crowley, L.B. Ricchetti, C.U. Pittman Jr, R. Anderson, T.E. Mlsna, Rapid removal of salicylic acid, 4-nitroaniline, benzoic acid and phthalic acid from wastewater using magnetized fast pyrolysis biochar from waste douglas fir, Chem. Eng. J. 319 (2017) 75–88.
- [32] C. Peng, J. Dai, J. Yu, J. Yin, Calcined Mg-Fe layered double hydroxide as an absorber for the removal of methyl orange, AIP Adv. 5 (5) (2015) 057138.
- [33] S. Chang, M. Jackson, Solubility product of iron phosphate 1, Soil Sci. Soc. Am. J. 21 (3) (1957) 265–269.
- [34] T. Daou, S. Begin-Colin, J. Greneche, F. Thomas, A. Derory, P. Bernhardt, P. Legaré, G. Pourroy, Phosphate adsorption properties of magnetite-based nanoparticles, Chem. Mater. 19 (18) (2007) 4494–4505.

- [35] C.M. Navarathna, N. Bombuwala Dewage, C. Keeton, J. Pennisson, R. Henderson, B. Lashley, X. Zhang, E.B. Hassan, F. Perez, D. Mohan, Biochar adsorbents with enhanced hydrophobicity for oil spill removal, ACS Appl. Mater. Interfaces 12 (8) (2020) 9248–9260.
- [36] I. Ahmed, M. Gasser, Adsorption study of anionic reactive dye from aqueous solution to Mg-Fe-CO3 layered double hydroxide (LDH), Appl. Surf. Sci. 259 (2012) 650-656.
- [37] N.B. Dewage, A.S. Liyanage, C.U. Pittman Jr, D. Mohan, T. Mlsna, Fast nitrate and fluoride adsorption and magnetic separation from water on α-Fe2O3 and Fe3O4 dispersed on Douglas fir biochar, Bioresour. Technol. 263 (2018) 258– 265
- [38] D. Pani, S. Montinaro, E. Trainito, G. Cao, Caves and protected areas in sardinia (IT): the example of the Grotta del Papa cave system in the isle of tavolara, in: 16th International Congress of Speleology, 2013, pp. 370.
- [39] J.P. Popić, B.V. Jegdić, J.B. Bajat, M. Mitrić, V.B. Mišković-Stanković, Surface coverage determination of iron-phosphate coatings on steel using voltammetric anodic dissolution technique, J. Serb. Chem. Soc. 78 (1) (2013) 101–114.
- [40] R. Lin, A.P. Amrute, F. Krumeich, K. Lázár, R. Hauert, M. Yulikov, J. Pérez-Ramírez, Phase-controlled synthesis of iron phosphates via phosphation of β-FeOOH nanorods, CrystEngComm 18 (18) (2016) 3174–3185.
- [41] J. Alchouron, C. Navarathna, H.D. Chludil, N.B. Dewage, F. Perez, C.U. Pittman Jr, A.S. Vega, T.E. Mlsna, Assessing South American Guadua chacoensis bamboo biochar and Fe3O4 nanoparticle dispersed analogues for aqueous arsenic (V) remediation, Sci. Total Environ. 706 (2020) 135943.
- [42] Ä. Sällsk, Är analyses according to the Debye Scherrer method. I, The cubic system, Kungl, Acta Universitatis Lundensis: Lunds universitets årsskrift 31 (1895).
- [43] H. El Ghandoor, H. Zidan, M.M. Khalil, M. Ismail, Synthesis and some physical properties of magnetite (Fe₃O₄₎ nanoparticles, Int. J. Electrochem. Sci. 7 (6) (2012) 5734–5745.
- [44] I.G. Richardson, Clarification of possible ordered distributions of trivalent cations in layered double hydroxides and an explanation for the observed variation in the lower solid-solution limit, Acta Crystallograph. Sect. B: Struct. Sci. Crystal Eng, Mater. 69 (6) (2013) 629–633.
- [45] K. Parida, L. Mohapatra, Carbonate intercalated Zn/Fe layered double hydroxide: a novel photocatalyst for the enhanced photo degradation of azo dyes, Chem. Eng. J. 179 (2012) 131–139.
- [46] K. Parida, M. Satpathy, L. Mohapatra, Incorporation of Fe 3+ into Mg/Al layered double hydroxide framework: effects on textural properties and photocatalytic activity for H 2 generation, J. Mater. Chem. 22 (15) (2012) 7350–7357.
- [47] D. Angin, S. Şensöz, Effect of pyrolysis temperature on chemical and surface properties of biochar of rapeseed (Brassica napus L.), Int. J. Phytorem. 16 (2014) 684–693.
- [48] C. Luengo, M. Brigante, J. Antelo, M. Avena, Kinetics of phosphate adsorption on goethite: comparing batch adsorption and ATR-IR measurements, J. Colloid Interface Sci. 300 (2) (2006) 511–518.
- [49] C.M. Navarathna, A.G. Karunanayake, S.R. Gunatilake, C.U. Pittman Jr, F. Perez, D. Mohan, T. Mlsna, Removal of Arsenic (III) from water using magnetite precipitated onto Douglas fir biochar, J. Environ. Manage. 250 (2019) 109429.
- [50] W.-G. Hou, Y.-L. Su, D.-J. Sun, C.-G. Zhang, Studies on zero point of charge and permanent charge density of Mg-Fe hydrotalcite-like compounds, Langmuir 17 (6) (2001) 1885–1888.
- [51] S. Prasanna, P.V. Kamath, Anion-exchange reactions of layered double hydroxides: interplay between coulombic and H-bonding interactions, Ind. Eng. Chem. Res. 48 (13) (2009) 6315–6320.
- [52] I. Langmuir, The adsorption of gases on plane surfaces of glass, mica and platinum, I. Am. Chem. Soc. 40 (9) (1918) 1361–1403.
- [53] H. Freundlich, Over the adsorption in solution, J. Phys. Chem. 57 (385471) (1906) 1100–1107.
- [54] S. Wan, S. Wang, Y. Li, B. Gao, Functionalizing biochar with Mg–Al and Mg–Fe layered double hydroxides for removal of phosphate from aqueous solutions, J. Ind. Eng. Chem. 47 (2017) 246–253.
- [55] L.-G. Yan, K. Yang, R.-R. Shan, T. Yan, J. Wei, S.-J. Yu, H.-Q. Yu, B. Du, Kinetic, isotherm and thermodynamic investigations of phosphate adsorption onto core-shell Fe3O4@ LDHs composites with easy magnetic separation assistance, J. Colloid Interface Sci. 448 (2015) 508–516.
 [56] S.K. Milonjić, A consideration of the correct calculation of thermodynamic
- [56] S.K. Milonjić, A consideration of the correct calculation of thermodynamic parameters of adsorption, J. Serb. Chem. Soc. 72 (12) (2007).
- [57] B. Monárrez-Cordero, A. Sáenz-Trevizo, L. Bautista-Carrillo, L. Silva-Vidaurri, M. Miki-Yoshida, P. Amézaga-Madrid, Simultaneous and fast removal of As³⁺, As⁵⁺, Cd²⁺, Cu²⁺, Pb²⁺ and F⁻ from water with composite Fe-Ti oxides nanoparticles, J. Alloys Compd. 757 (2018) 150–160.
- [58] D. Mohan, P. Singh, A. Sarswat, P.H. Steele, C.U. Pittman Jr., Lead sorptive removal using magnetic and nonmagnetic fast pyrolysis energy cane biochars, J. Colloid Interface Sci. 448 (2015) 238–250.
- [59] M. Zhang, B. Gao, Y. Yao, Y. Xue, M. Inyang, Synthesis of porous MgO-biochar nanocomposites for removal of phosphate and nitrate from aqueous solutions, Chem. Eng. J. 210 (2012) 26–32.
- [60] K.-W. Jung, K.-H. Ahn, Fabrication of porosity-enhanced MgO/biochar for removal of phosphate from aqueous solution: application of a novel combined electrochemical modification method, Bioresour. Technol. 200 (2016) 1029– 1032.

- [61] J. Jack, T.M. Huggins, Y. Huang, Y. Fang, Z.J. Ren, Production of magnetic biochar from waste-derived fungal biomass for phosphorus removal and recovery, J. Cleaner Prod. 224 (2019) 100–106.
- [62] K.-W. Jung, T.-U. Jeong, M.-J. Hwang, K. Kim, K.-H. Ahn, Phosphate adsorption ability of biochar/Mg-Al assembled nanocomposites prepared by aluminum-electrode based electro-assisted modification method with MgCl2 as electrolyte, Bioresour. Technol. 198 (2015) 603–610.
- [63] R. Li, J.J. Wang, B. Zhou, M.K. Awasthi, A. Ali, Z. Zhang, L.A. Gaston, A.H. Lahori, A. Mahar, Enhancing phosphate adsorption by Mg/Al layered double hydroxide functionalized biochar with different Mg/Al ratios, Sci. Total Environ. 559 (2016) 121–129.
- [64] E.M. Seftel, R.G. Ciocarlan, B. Michielsen, V. Meynen, S. Mullens, P. Cool, Insights into phosphate adsorption behavior on structurally modified ZnAl layered double hydroxides, Appl. Clay Sci. 165 (2018) 234–246.
- [65] L.-G. Yan, K. Yang, R.-R. Shan, T. Yan, J. Wei, S.-J. Yu, H.-Q. Yu, B. Du, Kinetic, isotherm and thermodynamic investigations of phosphate adsorption onto core-shell Fe3O4@LDHs composites with easy magnetic separation assistance, J. Colloid Interface Sci. 448 (2015) 508–516.
- [66] R. Chitrakar, S. Tezuka, A. Sonoda, K. Sakane, K. Ooi, T. Hirotsu, Adsorption of phosphate from seawater on calcined MgMn-layered double hydroxides, J. Colloid Interface Sci. 290 (1) (2005) 45–51.
- [67] A.G. Karunanayake, C. Navarathna, S. Gunatilake, M. Crowley, R. Anderson, D. Mohan, F. Perez, C.U. Pittman, T.E. Mlsna, Fe3O4 nanoparticles dispersed on Douglas Fir Biochar for phosphate sorption, ACS Appl. Nano Mater. (2019).
- [68] Y. Ma, Y. Wang, D. Xie, Y. Gu, X. Zhu, H. Zhang, G. Wang, Y. Zhang, H. Zhao, Hierarchical MgFe-layered double hydroxide microsphere/graphene composite for simultaneous electrochemical determination of trace Pb (II) and Cd (II), Chem. Eng. J. 347 (2018) 953–962.